Materials Science and Engineering B 177 (2012) 1452–1459

Contents lists available at SciVerse ScienceDirect

Materials Science and Engineering B

journal homepage: www.elsevier.com/locate/mseb

Structural and optical characterization of mechanochemically synthesized copper doped CdS nanopowders

P. Reyes*, S. Velumani

Departamento de Ingeniería Eléctrica-SEES, CINVESTAV-IPN, Zacatenco, D.F., C.P.07360, México, Mexico

ARTICLE INFO

Article history:
Received 1 October 2011
Received in revised form 18 February 2012
Accepted 3 March 2012
Available online 28 March 2012

Keywords:
Cu doped CdS
Ball milling
Nanopowder
HRTEM

ABSTRACT

Incorporation of copper into CdS crystals has been successfully prepared by mechanical alloying using a planetary ball mill. The powders are prepared with different milling times at 300 rpm with various Cu/Cd ratios from 0.1 to 25 at%. X-ray diffraction (XRD) analysis of milled powders showed peaks corresponding to hexagonal structure with a detection of phase transition to a cubic structure with increasing milling time. Grain sizes varied from 21 to 30 nm corresponding to different Cu/Cd ratios. Field emission scanning electron microscopy (FESEM) images reveal agglomerated materials with particle size of approximately 28 nm (5 Cu at%) and layered structures caused due to the milling process. Powder composition by energy dispersive analysis of X-rays (EDAX) reveals the incorporation of copper into the CdS. Micro Raman spectroscopy showed peaks approximately at 301 and 585 cm^{-1} corresponding to first and second order scatterings of longitudinal optical phonon mode. The LO mode at 301 cm^{-1} shifted towards lower wave number due to decrease of grain size by increase in milling time. From high resolution transmission electron microscope (HRTEM), the dominant phase of individual CdS nanocrystals was found to be hexagonal structure along with cubic structure.

1. Introduction

CdS is a II–VI n-type semiconductor with a direct band-gap of 2.42 eV and a hexagonal (stable) or cubic (metastable) structure. It has applications in laser materials, photo resistance, light emitting diode, nonlinear optical devices, etc. It is widely used as window material for solar cells [1]. Two basic requirements for the window material are the low electrical resistivity and high optical transmittance. An effective way to obtain CdS with these requirements can be achieved by the creation of Cd excess or S vacancies [2] with the incorporations of different impurities such as Cu [3], Fe [4] Ag [5], Al [6] and Ga [7]. Copper impurities behave as an acceptor in CdS, changing the resistivity, bandgap energy, photoelectrical properties [3] and also changing the type of semiconductor from n to p (useful for CdS:Cu/CdS PV devices) [3].

Many methods have been used to incorporate dopants into CdS, some of these methods are: ion-exchange reaction [8], dry process [9], spray pyrolysis [10], and vacuum deposition [11]. Mechanical alloying (MA) can be considered as a simple, inexpensive and novel alternate process to obtain CdS with various Cu concentrations. MA is a solid-state processing technique that involves welding, fracturing and rewelding of powder particles at atomic level [12], capable of synthesizing a variety of stable and metastable alloy phases [13]. Some of the important parameters that have an effect on the final constitution of the powder are the milling speed, milling time and ball-to-powder weight ratio. The milling time is an important parameter and normally it is chosen to achieve a steady state between the fracturing and cold welding of the powder particles. The samples obtained from mechanical alloying are polycrystalline with aggregates of crystallites forming grains with grain boundaries. The structure of the powders influences all its optoelectronic and optical properties. As an example, the photoconductivity response in polycrystalline materials composed of several microcrystallites has an additional adsorption band beyond the band edge. This band is related with the decrease in crystalline size [6].

Different systems have been obtained by mechanochemical synthesis reactions. Experiments reported by Suryanarayana [12] shows successfully achieved reactions on binary and ternary compounds related with copper and aluminum (CuO, CuO + Al) using 2 h milling time. Taking this into consideration, we decided to use milling times equal or higher than 2 h. The prepared CdS nanoparticle powder can be deposited in films by spraying, curtain coating, roll coating, doctor blading, or screen-printing [13] for applications in low-cost thin-film solar cells or thin photoconductive layers.

Although there are some reports on Cu doped CdS [3,11,14], so far to our knowledge this is the first attempt to make Cu doped CdS through mechanochemical alloying. Hence this paper focuses on the preparation and structural characterization of Cu doped CdS nanoparticles obtained by a simple mechanochemical route

* Corresponding author. Tel.: +52 55 5747 4001; fax: +52 55 5747 4003.
E-mail addresses: pireyes@cinvestav.mx, itzam29@gmail.com (P. Reyes).

0921-5107/$ – see front matter © 2012 Elsevier B.V. All rights reserved.
doi:10.1016/j.mseb.2012.03.002

using high-energy milling. The incorporation and influence of copper dopants on surface morphology, composition analysis, Raman spectroscopy and microstructure were investigated and reported. Besides, we have explored the effect of the milling time on the preparation of nanopowders.

2. Experimental details

Cu doped CdS nanopowders were synthesized by mechanical alloying using Retsch PM400 planetary ball mill, mixing high purity precursors of Copper (Sigma–Aldrich granulate Cu 99.9% pure, particle diameter 422–2000 μm) and CdS powder (Sigma–Aldrich 99.99% pure), using tungsten carbide vial and balls. In order to prevent or minimize the powder contamination from oxygen [12], the powders were sealed in vials under nitrogen (N_2) atmosphere. Millings of the powders were carried out at 300 rpm, keeping ball-to-powder ratio as 5:1 for 2 and 3 h with various Cu/Cd ratios of 0.1, 1, 5 and 25 at% (atomic percentage). The structure of milled powders was examined using a Philips XPERT-PRO system with a Cu Kα (λ = 1.54051 Å) radiation. The diffraction angle was varied from 20° to 75°, and the Miller index (*h k l*) obtained from the diffraction spectra were identified using Joint Committee on Powder Diffraction Standards (JCPDS) cards (ICSD #: 067776). Raman measurements were carried out using an Olympus BX41 Horiba Jobin Yvan micro-Raman system with He–Ne laser wavelength of 632 nm with a power of 20 mW. HRTEM analysis was performed using a FEI Tecnai F30 transmission electron microscope with beam energy of 300 kV. Composition and morphology of the nanopowders were determined using Carl Zeiss Auriga Field Emission Scanning Electron Microscope (FESEM) accompanied with Bruker Energy Dispersive Analysis of X-ray (EDAX) system.

3. Results and discussion

3.1. Structural analysis

After the milling process, the colour of the CdS samples changed from yellow to dark orange with different copper concentrations, which may be due to the work-damage and the reduction of particle size as noticed by Durose et al. [13] and Tsuzuki and McCormick [15] for milled CdS powders. Fig. 1 shows the XRD pattern of pure CdS powder where all diffraction peaks corresponds to those of hexagonal CdS (ICSD #: 067776 also in figure).

Fig. 2(a) and (b) shows the diffraction patterns of mechanical alloyed Cu doped CdS powder with a Cu/Cd ratio of 0.1 at%, 1 at%, 5 at% and 25 at%. All the XRD graphs of CdS:Cu are in accordance with the hexagonal structure of CdS. Meanwhile, the (0 0 2) peak shows a considerable increase in intensity upon incorporation of Cu. This behavior of doped CdS was observed by others [6] and could be attributed to the change in the scattering factor corresponding to the incorporated element, or the decrease in the crystallite size, or both. The grain size was determined from XRD spectrum using the Scherer formula:

$$D = \frac{0.94\lambda}{\beta \cos \theta}$$

where D is crystal size, λ is the wavelength of the X-ray, β is full width at half maximum (FWHM) and θ is Bragg's angle. The size of CdS:Cu grains was calculated from an average of all diffraction peaks. Variation from 21 to 30 nm corresponds to the change in Cu/Cd ratio. Full widths at half maximum (FWHMs) of the XRD peaks for 1 Cu at% were smaller than those of 0.1 Cu at%, and they were further decreased by increasing Cu content. This result shows that the grain growth of CdS was promoted by Cu incorporation, increasing the size from 21 to 30 nm for 0.1 to 25 Cu at% respectively (see Table 2). In Fig. 2(b), a shift to the right is observed

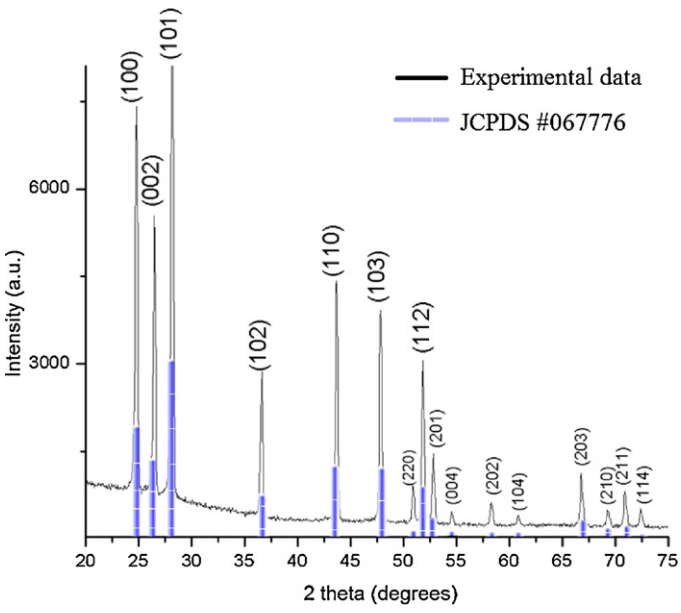

Fig. 1. X-ray diffraction pattern of pure CdS powder (before milling) showing hexagonal structure, compared with standard ICSD #: 067776 of CdS.

Table 1
EDAX analysis composition of Cu doped CdS nanopowders.

Sample	Percentage of copper doped (at%)	Cd (at%)	S (at%)	Cu (at%)
CdS:Cu1	0.1	52.06	47.94	–
CdS:Cu2	1	51.02	47.90	1.08
CdS:Cu3	5	49.30	47.93	2.77
CdS:Cu4	25	32.02	45.95	22.03

with increased Cu concentration. This shift can be a consequence of the incorporation of Cu into the Cd lattice. The smaller atomic radius of Cu (1.35 Å) as compared with that of Cd (1.51 Å) can be the cause of a structure shrinkage [16]. This can only happen if Cu atoms enter substitutionally into Cd sites. No diffraction peak of the copper (1 1 1) plane is observed at $2\theta = 43.54°$ (Fig. 2(a)) in the tail of the (1 1 0) CdS:Cu peak. No peaks other than those of CdS were observed. Therefore, XRD traces of crystalline Cu–S compounds such as Cu_2S could not be detected. The mapping analysis of CdS sample doped with 5 at% of copper (Fig. 3(a)) shows the presence of Cu all over the region, with some agglomeration of it (brighter zone) on the bottom left corner in the inset figure of Fig. 3(a). This kind of agglomeration is reported for other materials synthesized by this technique [17] and can be related to the mechanical alloying process. Fig. 3(b) and (c) shows the EDAX spectra of CdS:Cu powders with Cu concentration of 1 and 5 at%, with intense peaks confirming once again the content of copper in the samples. Regarding to the chemical state of copper in the doped CdS samples, XPS measurements carried out by Abe et al. [14] shows Cu $2p_{3/2}$ energy peaks of each spectrum are at approximately 932 eV. However, the binding energies of Cu metal, CuS and Cu_2S are 932.6, 932.2 and 932.5 eV, respectively [18]. Therefore, it is very difficult to determine the chemical states of Cu since electrical charging by strong irradiation of X-rays during EDAX measurements may cause change in surface potential. Further deposition of CdS:Cu nanopowders is needed in order to measure electrical properties which help to recognize, how Cu doping is taking place.

In this work, not only the minimum particle size is desired for further studies and applications but also the maximum incorporation of the dopant material. For this reason, the milling time was varied in order to substantiate our goal. Hence, Fig. 4 shows

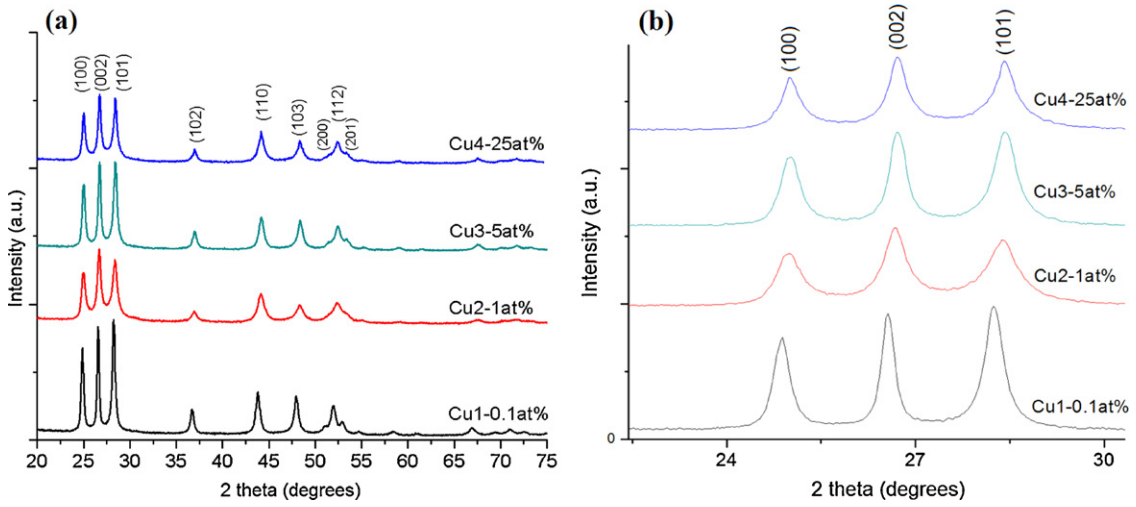

Fig. 2. (a) XRD pattern of Cu doped CdS nanopowders with different Cu/Cd ratios and (b) extended 2θ graph of (a).

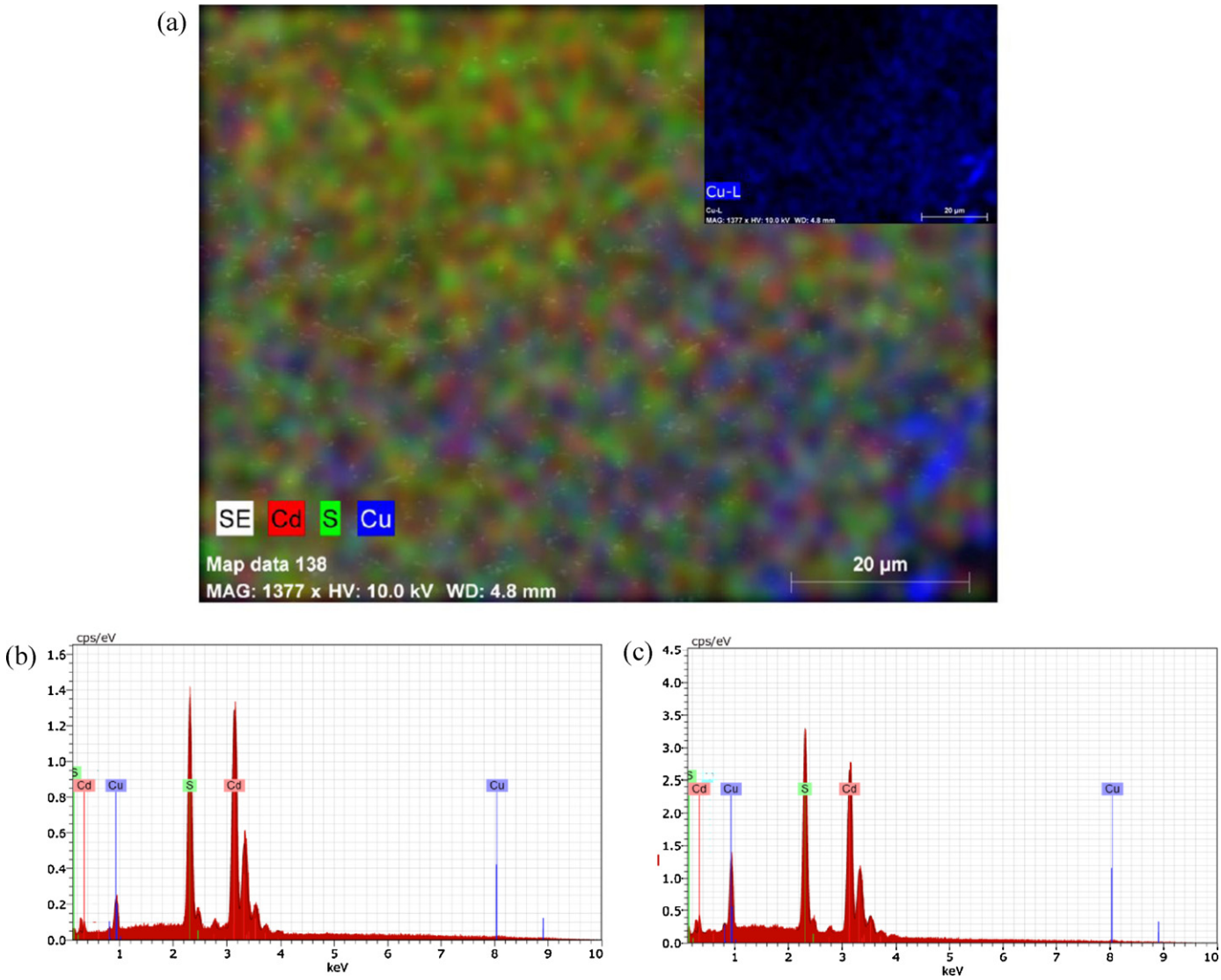

Fig. 3. EDAX analysis, (a) mapping of Cu 5 at%. (b) EDAX spectra of Cu 1 at% and (c) 5 at%.

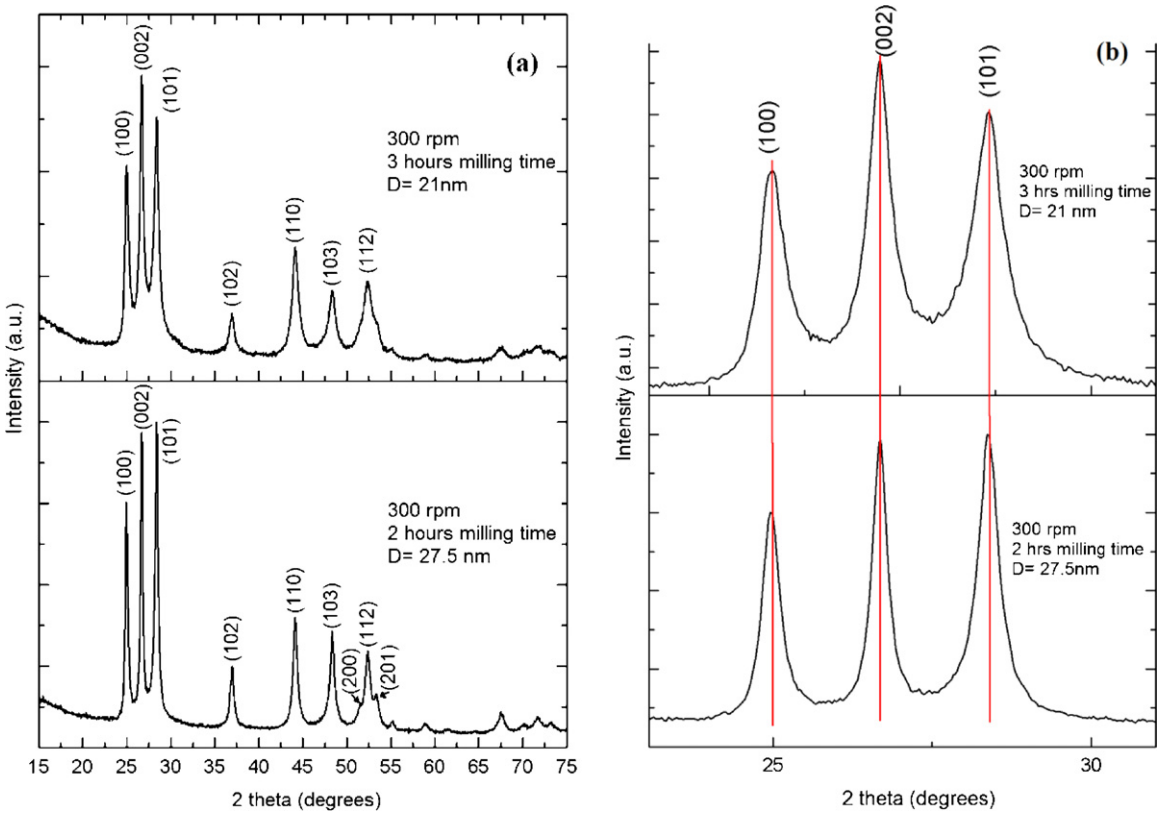

Fig. 4. (a) X-ray diffractograms of 1 at% Cu/Cd ratio for 2 and 3 h milling time and (b) broadening of peaks with increasing milling time.

the effect of milling time (2 h and 3 h) on the CdS:Cu XRD pattern with Cu/Cd ratio of 1. Table 3 gives a comparison of crystalline size which decrease with increasing milling time (27.55–20.36 nm). These sizes are improved in comparison with Durose et al. [13] where a crystalline size of 500 nm is obtained after a 0.5 h milling. The difference in crystalline size can be attributed to the use of high energy ball milling and higher times. Two and three hours samples had (1 0 0), (0 0 2), (1 0 1), (1 0 2), (1 1 0), (1 0 3), etc., planes corresponding to hexagonal structure. For 2 h CdS:Cu (2 0 0), (1 1 2) and (2 0 1) planes from hexagonal structure are identified. For 3 h milling time (1 1 2) plane is observed with (2 0 0) and (2 0 1) planes decreased in intensity (Fig. 4(a)). With higher milling time values, (2 0 0) and (2 0 1) planes are expected to totally disappear [13], although the (1 1 2) reflections remain. This is similar to the type of change widely reported for milled ZnS [19–21] and for polished CdS, CdSe and ZnS surfaces [22], which has usually been attributed to a transformation to the cubic phase.

When a powder is subjected to mechanical alloying, change in the structure occurs, which is manifested in the XRD as a change from hexagonal to more cubic-like diffraction pattern [13]. This change is attributed to introduction of disorder through the movement of dislocations during the mill process. Broadening of peaks in XRD is due to the reduction in the size of particles [13], decreasing from 27.55 nm to 21.05 nm is observed with increasing milling time for 2 and 3 h respectively (Fig. 4(b)). Also there is no left shift of peaks were observed which is normally dedicated to strain incorporated with increasing milling time, hence we can emphatically say that the strain incorporation is negligible in our technique which will yield good homogenous films for PV device fabrication.

3.2. Surface morphology and composition analysis

Using a field emission scanning electron microscopy (FESEM), morphology of the milled Cu doped CdS nanopowders was analyzed. Fig. 5 shows images of un-doped-un-milled and Cu doped-CdS nanopowders. The un-doped-un-milled powders mainly consist of hexagonal-like structures, matching with XRD pattern, whilst milled samples are agglomerated with no particular shape observable by SEM. But the HRTEM results indicate the presence of hexagonal structures. As shown in Fig. 5(b)–(e), a strong aggregation of particles is observed in milled samples, consequence of the mechanochemical synthesis, where particle size between 20 nm and 30 nm was observed (Fig. 5(f)). Table 1 shows the EDAX analysis of CdS:Cu powders. The atomic concentration of S is about 48%, and it is almost constant. The concentration of Cd is 52 at% at pure CdS, and decrease with Cu doping, although the total concentration of Cd and Cu is about 52 at% in the powders. Decrease in cadmium concentration is due to Cu acceptor incorporation into the CdS lattice in which Cd is substituted by Cu in unit cells. Powder particles during mechanical alloying are subjected to high energy

Table 2
Crystalline size of 3 h milled Cu doped CdS nanopowders.

Percentage of copper doped in CdS (at%)	Crystalline size (nm)
Pure CdS	20.36
0.1	21.05
1	24.90
5	27.25
25	29.45

Table 3
Crystalline size comparison of pure CdS powders milled at different times.

Milling time (h)	Crystalline size (nm)
0.5[a]	500
2	27.55
3	20.36

[a] Experiment carried out by Durose et al. [13].

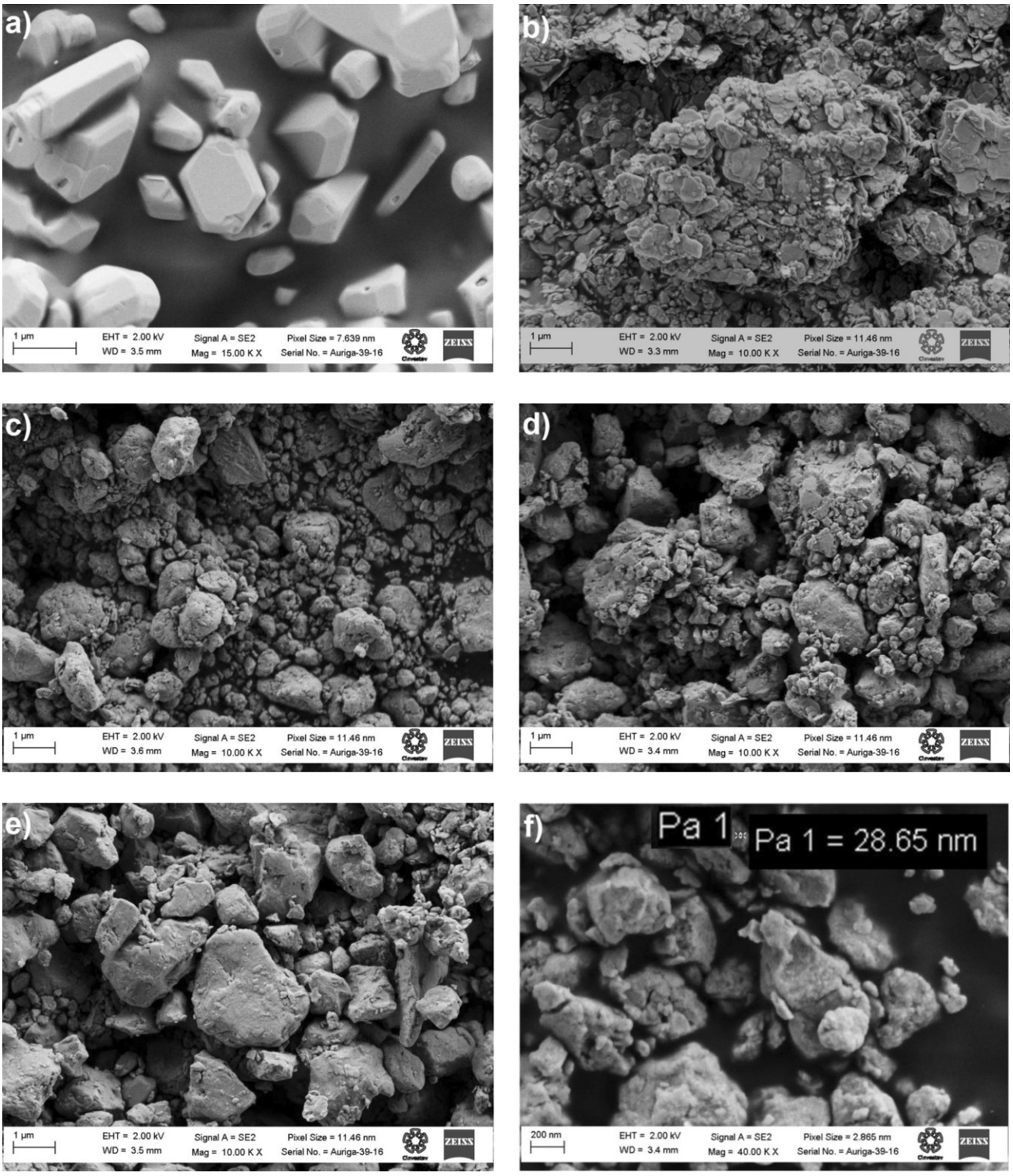

Fig. 5. SEM images of CdS nanopowders: (a) undoped-unmilled, (b) 0.1 at%, (c) 1 at%, (d) 5 at%, (e) 25 at% copper doped and (f) nanoparticle measurement of 5 at% sample.

collisions [23], which cause them to be cold welded together and fractured. This enables the powder particles to be always in contact with each other with atomically clean surfaces and with minimized diffusion distance. Diffusion is a fundamental process during the mechanical alloying [24], which helps the incorporation of Cu into the CdS. Substitutional Cu atoms diffuse by a vacancy mechanism where the activation energy for diffusion is equal to the sum of the activation energy to form the Cd vacancy and that to move the vacancy. In this regard, the activation energy for diffusion of Cu is lowered by reducing the activation energy needed for the creation of Cd vacancies and this is achieved by mechanical alloying with the formation of more free surfaces, grain boundaries and sub-grain boundaries [25].

At the particular milling time (3 h) used in this work, the doping of copper into cadmium sites is more difficult to control at higher Cu contents, which may be caused by the lack of new surfaces necessary for the diffusion of Cu into Cd sites. The diffusion mechanism in mechanical alloying differs from steady diffusion,

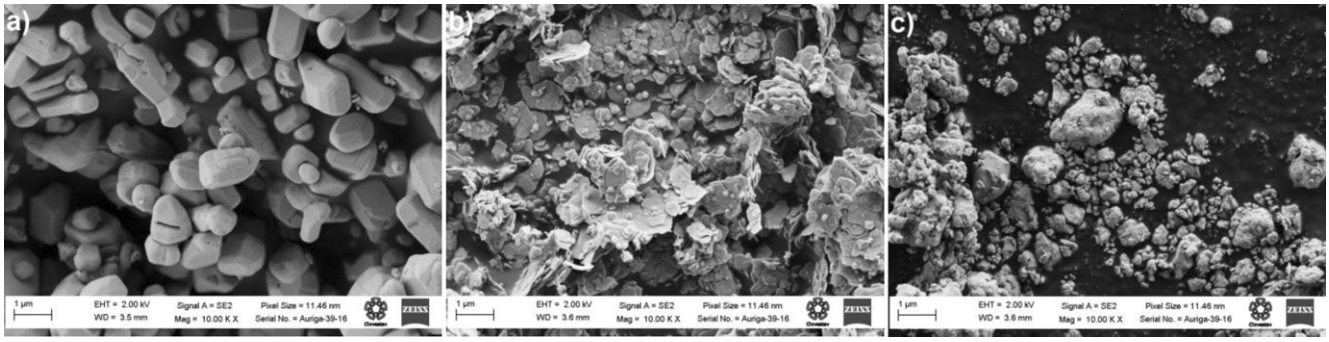

Fig. 6. SEM images of CdS powder under different milling time: (a) unmilled, (b) 2 and (c) 3 h milling time.

since the balance of atom concentration at the interface between different elements may be destroyed with subsequent fracturing of the powder particles. Consequently, new diffusion starts when the recently created surfaces (where composition may be very different) meet each other to form new diffusion couples when Cd, S and Cu powder particles are being welded together [24]. In this regard, may be a higher milling time is needed in order to create more new surfaces and enable the diffusion of more Cu into the structure.

In order to understand the effect of milling time on particle size and composition of 5 at% Cu/Cd powder, an evidence of the different steps involved in mechanochemical synthesis process is needed. The morphology obtained from FESEM image is a useful tool for this purpose. During milling, the powder particles are repeatedly flattened, cold welded, fractured and re-welded. The force of the impact, plastically deforms the powder particle precursors (Fig. 6(a)) leading to work hardening and fracture. Since in the early stages of milling, particles are soft, their tendency to weld together and form large particles is high. The composite particles at this stage have a characteristic layered structure (Fig. 6(b)). With continued deformation, the particles get work hardened and fracture by the fragmentation of fragile flakes. Fragments generated by this mechanism may continue to reduce in size. Due to the continued impact of grinding balls, the structure of the particles is steadily refined (Fig. 6(c)) [26]. In this regard, at 2 h milling time, the process is in a middle stage with the presence of flakes structures which are not optimum for obtaining nanoparticles powders. For 3 h milling time, more refined particles are observed and also smaller particle size is obtained.

3.3. HRTEM characterization

For structure analysis, apart from XRD, HRTEM is a useful analytical technique to identify particle size, type of structures, plane of orientation, induced morphologies, aggregation of nanoparticles and defects present in the sample [27–29]. Based on the XRD diffractograms, at 2 h milling time all the planes corresponds to hexagonal structure of the CdS, At this point, there is no evidence of phase transition from hexagonal to cubic structure. Sample milled at 3 h shows a phase transition when (2 0 0) and (2 0 1) peaks started to vanish and only (1 1 2) plane is left. Thus, it is more probable to find cubic CdS phase in powder milled at 3 h than the 2 h milled sample. To carry on the measurements, the 3 h milled 5 at% Cu/Cd sample were used. As shown in Fig. 7(a), HRTEM micrograph reveals agglomeration of nanoparticles which are composed of lots of small nanocrystal grains. Inserted in Fig. 7(b) are their fast Fourier transformations (FFT) and inverse fast Fourier transformation (IFFT) images. From this, the particles were identified to be hexagonal (wurtzite) structure and cubic (sphalerite) structure. Particle A has hexagonal structure exhibiting lattice planes (2 0 2), (2 0 1), (2 0 0) and (1 1 0) with d spacing of 1.557 Å, 1.732 Å, 1.782 Å and 2.079 Å. Particle B is identified to have mixed cubic/hexagonal structure exhibiting cubic lattice planes (4 0 0), (2 0 0) with d spacing of 1.459 Å and 2.932 Å respectively; and hexagonal lattice plane (2 0 0) with d spacing of 1.775 Å. A similar phase transition is observed for CdSe and CdS nanoparticles synthesized using mechanical alloying process by Tan et al. [30,31]. The phase transition may be induced by high pressure impacting on the powders from the ball against

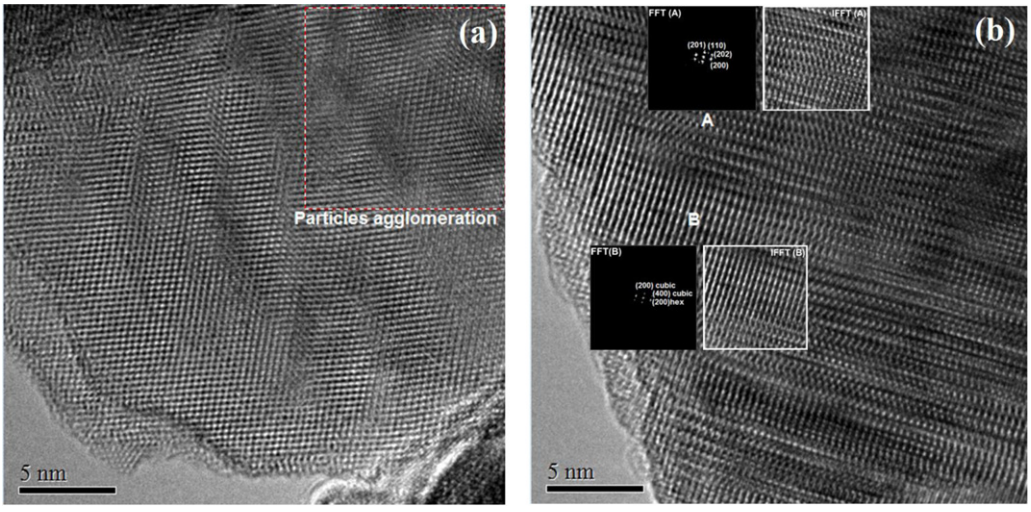

Fig. 7. HRTEM images of (a) agglomerated milled CdS nanoparticles and (b) sample showing mixture phase of hexagonal and cubic structures, doped with 5 at% of copper.

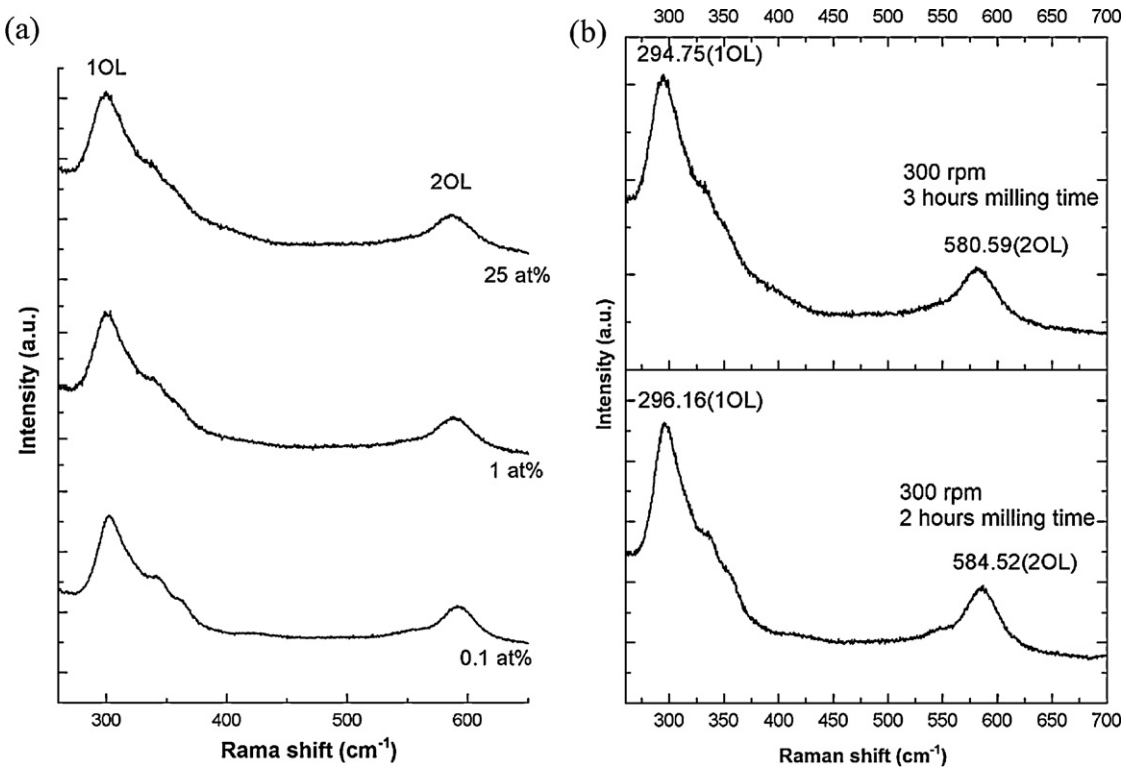

Fig. 8. Raman spectroscopy of CdS:Cu with (a) different Cu/Cd ratios, (b) different milling time for 1 at% Cu doped CdS.

the wall during the high frequency rotation movement of the vial [30]. Progressive change from the expected hexagonal to a more cubic-like structure due to mechanical alloying is observed by others authors [32].

3.4. Micro-Raman spectroscopy

The Raman spectra of the CdS:Cu nanoparticles given in Fig. 8(a) present a well resolved line at approximately 301 cm^{-1} and 585 cm^{-1}, corresponding to the first order scattering of the longitudinal optical (LO) phonon mode [33] and second-order scattering of LO phonons, respectively. Similar trend has been observed by Ma et al. [5] for CdS films prepared by ultrasound-assisted microwave. In addition, shoulders peak at approximately 340 and 365 cm^{-1}, could be related to defect-induced modes, disorder activated combination modes or local modes involving copper [33]. The peak at 301 cm^{-1} is asymmetric, suggesting a superposition of more than one mode. This peak consists of a superposition of three different peaks: cubic 1LO or hexagonal A1(LO)/E1(LO) peak. Raman spectra present well defined LO peaks, which broaden for samples with high concentration of copper indicating compositional disorder.

In Fig. 8(b) a milling time comparison is presented between 2 h and 3 h at a same Cu concentration of 1 at%. Positions of the peak shift towards lower wave number with decreasing grain size due to increased milling time [34]. This shift in frequency of the 1 LO Raman peak in CdS nanoparticles has been studied before and is mainly ascribed to the grain size effect. It is now known that confinement of phonons, optical as well as acoustic, influences the phonon spectra when the grain size falls to a few nanometers. Confinement of optical phonons causes a shift towards the low frequency side compared to that for bulk CdS (1 LO 301.5 cm^{-1}) [34].

Fig. 9 displays the reflectance (R) curves for undoped and 1, 5, 15 at% Cu doped CdS powders milled for 3 h. The figure indicates that there is an appreciable shift in the absorption edge towards the longer wavelength side for the CdS:Cu samples. This result indicates a change in the optical band gap of the powder after Cu doping. The optical band gap calculated from α^2 versus $h\nu$ plot is shown in Table 4. This shows the decrease in the band gap of the CdS powder from about 2.28 to 1.96 eV after Cu doping.

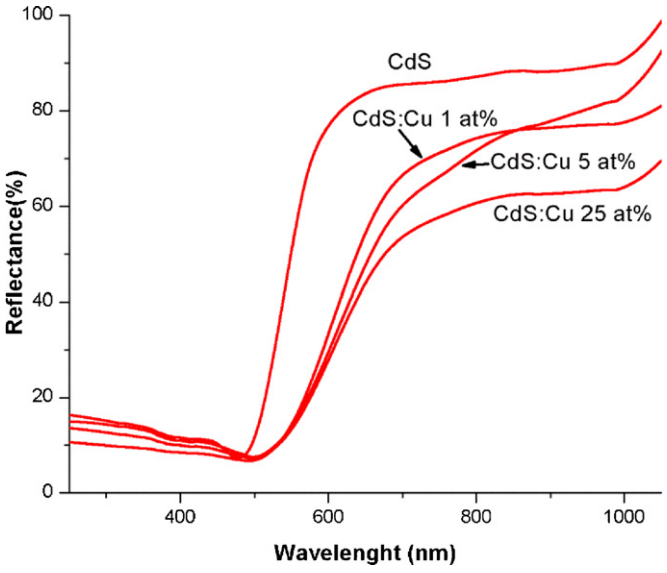

Fig. 9. The effect of Cu doping on the reflectance of CdS powders.

Table 4
Optical band gap of Cu doped CdS nanopowders.

Sample	Percentage of copper doped	Optical band gap (eV)
CdS	–	2.28
CdS:Cu2	1	2.02
CdS:Cu3	5	2.00
CdS:Cu4	25	1.96

4. Conclusions

Cu doped CdS nanoparticles are successfully prepared by fast, simple and safe technique using mechanochemical process. XRD showed polycrystalline nature of Cu doped CdS exhibiting (2 0 0) and (2 0 1) peaks which are associated to hexagonal phase. These peaks diminished with increasing milling time due to the introduction of disorder through the movement of dislocations during the milling process. The nonappearance of peak at 43.54° corresponding to pure copper and the peak shifting after Cu doping, infers the safe incorporation of Cu into CdS lattices. From FESEM images particle size are found to be 28 nm. FESEM images also revealed the agglomeration and flake structures which are due to the mechanical alloying process. From EDAX analysis the percentage of copper in CdS was evaluated and found to be close to the initial precursors added. HRTEM images revealed agglomerated nanoparticles composing of lots of small nanocrystal grains with the presence of hexagonal and cubic phases which is also identified from Raman spectra. LO peaks in Raman spectra broadened for samples with high concentration of copper indicating compositional disorder. Decrease in optical band gap of Cu doped CdS from 2.28 to 1.96 eV indicates the incorporation of Cu in the CdS structure. The XRD, FESEM, HRTEM, Raman spectra and optical analysis prove the incorporation of copper into CdS lattices by this simple technique.

Acknowledgments

We thank Mr. Alvaro Angeles Pascual and Mr. Josue at Laboratorio Nacional de Microscopia Electronic de Alta Resolusión, Cinvestav for the FESEM and EDAX facilities and to Dr. Miguel Avalos of LINAN, IPICYT, San Luis Potosi for their help in HRTEM analysis.

References

[1] A. Irajizad, R.M. Tilaki, S.M. Mahdavi, Scientia Iranica 15 (2008) 360–365.
[2] S. Mathew, P. Mukerjee, K. Vijayakumar, Japanese Journal of Applied Physics 34 (1995) 4940–4944.
[3] Y. Kashiwaba, K. Isojima, K. Ohta, Solar Energy Materials & Solar Cells 75 (2003) 253–259.
[4] M. Thambidurai, N. Muthukumarasamy, S. Agilan, N. Murugan, N. Sabari, S. Vasanthe, R. Balasundaraprabhu, Solid State Science 12 (2010) 1554–1559.
[5] J. Ma, G. Tai, W. Guo, Ultrasonics Sonochemistry 17 (2010) 534–540.
[6] H.H. Afify, I.K. El Zawawi, I.K. Battisha, Journal of Material Science: Materials in Electronics 10 (1999) 497–502.
[7] H. Khallaf, G. Chai, O. Lupan, L. Chow, S. Park, A. Schulte, Applied Surface Science 25 (2009) 4129–4134.
[8] M. Ristova, M. Ristov, P. Tosev, M. Mitreski, Journal of Physical Chemistry 100 (1996) 13226–13239.
[9] C. Feldman, G. Deutscher, E. Grünbaum, Applied Surface Science 48-49 (1991) 535–539.
[10] V. Valdna, Solid State Phenomena 67–68 (1999) 309.
[11] Y. Kashiwaba, T. Komatsu, M. Nishikawa, Y. Ishikawa, K. Segawa, Y. Hayasi, Thin Solid Films 408 (2002) 43–50.
[12] C. Suryanarayana, Intermetallics 3 (1995) 60–153.
[13] K. Durose, A.T. Fellows, A.W. Brinkman, G.J. Russell, Journal of Materials Science 20 (1985) 3783–3789.
[14] T. Abe, Y. Kashiwaba, M. Baba, J. Imai, H. Sasaki, Applied Surface Science 175–176 (2001) 549–554.
[15] T. Tsuzuki, P.G. McCormick, Applied Physics A 65 (1997) 607–609.
[16] J.A. Dávila-Pintle, R. Lozada-Morales, R. Palomino-Merino, B. Rebollo-plata, C. Martinez-Hipati, O. Portillo-Moreno, S. Jimenez-Sandoval, O. Zelaya-Angel, Journal of Materials Online 2 (2006) 1–7.
[17] N. Benslima, S. Mehdaoui, O. Aissaoui, M. Benabdeslema, A. Bouasla, L. Bechiri, A. Otmani, X. Portier, Journal of Alloys and Compounds 489 (2010) 437–440.
[18] F. Moulder, W. Stickle, P. Sobol, K. Bomben, Physical Electronics Division (1992).
[19] A. Schlede, H.Z. Gantzchow, Physical Chemistry 106 (1993) 37.
[20] F. Smith, V. Hill, Acta Crystallographica 9 (1956) 821.
[21] T. Sekine, Y. Kotera, Journal of Luminescence 12/13 (1976) 929.
[22] G.J. Russell, A.T. Fellows, S. Oktk, I.E. Ture, J. Woods, Journal of Materials Science Letters 176 (1982).
[23] J.S. Benjamin, Proceedings of the Novel Powder Metallurgy Worm Congress (1992) 155–168.
[24] L. Lu, M.O. Lai, S. Zhang, Journal of Materials Processing Technology 67 (1997) 100.
[25] L. Lu, Material Design 16 (1994) 33–39.
[26] C. Suryanarayana, Prodress in Materials Science 46 (2001) 1–184.
[27] A. Asencio, C. Gutierrez-Wing, Surface Science 396 (1998) 349–369.
[28] H. Liu, U. Pal, Microscopy Research and Technique 69 (2006) 522–530.
[29] M. Jose-Yacaman, J.A. Ascencio, H. Liu, Journal of Vacuum Science and Technology B 19 (2001) 1091–1107.
[30] G. Tan, J. Dun, Q. Zhang, Journal of Alloys and Compounds 468 (2009) 421–431.
[31] G.L. Tan, L. Zhang, X.-F. Yu, Journal of Physical Chemistry C 114 (2010) 290–293.
[32] E. Dutkova, P. Balaz, P. Pourghahramani, S. Velumani, J.A. Ascencio, N.G. Kostova, Journal of Nanoscience and Nanotechnology 9 (2009) 1–6.
[33] G. Perna, V. Capozzi, M. Ambrico, V. Augelli, T. Ligonzo, A. Minafra, L. Schiavulli, M. Pallara, Thin Solid Films 453–454 (2004) 187–194.
[34] R. Prabhu, M. Al Khadar, Bulletin of Materials Science 31 (2008) 511–515.